


Four-electron negative- U vacancy defects in antimony selenideXinwei Wang¹,¹ Seán R. Kavanagh^{1,2},² David O. Scanlon^{1,2},² and Aron Walsh^{1,3,*}¹Thomas Young Centre and Department of Materials, Imperial College London, Exhibition Road, London SW7 2AZ, United Kingdom²Thomas Young Centre and Department of Chemistry, University College London, 20 Gordon Street, London WC1H 0AJ, United Kingdom³Department of Physics, Ewha Womans University, Seoul 03760, Korea (Received 7 February 2023; revised 2 June 2023; accepted 12 September 2023; published 4 October 2023)

The phenomenon of negative- U behavior, where a defect traps a second charge carrier more strongly than the first, has been established in many host crystals. Here, we report the case of four-carrier transitions for both vacancy defects in Sb_2Se_3 . A global structure searching strategy is employed to explore the defect energy landscape from first principles, revealing large atomic reconfigurations which facilitate a major charge redistribution. A thermodynamic analysis of the accessible charge states reveals a four-electron negative- U transition ($\Delta q = 4$) for both V_{Se} and V_{Sb} which, combined with previous calculations for antisites and interstitials, now demonstrates amphoteric behavior for *all* intrinsic point defects in Sb_2Se_3 , with an impact on its usage in solar cells. The unusual behavior is facilitated by valence alternation, a reconfiguration of the local bonding environments, characteristic of both Se and Sb.

DOI: [10.1103/PhysRevB.108.134102](https://doi.org/10.1103/PhysRevB.108.134102)**I. INTRODUCTION**

Point defects play a decisive role in the performance of semiconductor devices [1]. They are localized in real space and can act as charge traps. A defect can capture two charge carriers of the same type with a larger binding energy for the second than the first, if the stabilization energy (e.g., from structural relaxation and exchange interactions) compensates the on-site Coulomb repulsion energy between the two carriers [2,3]. This energy cost of trapping an *additional* charge carrier is defined as the Hubbard correlation energy (U) [4], and such a defect with negative correlation energy is termed a negative- U center. The concept of negative U was proposed by Anderson [5] to explain the preference of paired electrons in chalcogenide glasses and expanded by Street and Mott [6] to defects in the same materials. Kastner *et al.* [7] then proposed a valence-alternation model to account for the atomic reconstructions arising from dangling bonds. They noted that valence alternation is applicable to both amorphous and crystalline chalcogenides as well as materials with group-V atoms (e.g., As, Sb, Bi). Since then, negative- U behavior has been widely reported in systems including oxides, carbides, and compound semiconductors such as GaAs and CdTe. [8–12].

Antimony selenide (Sb_2Se_3) has emerged as an earth-abundant absorber layer for thin-film solar cells due to its promising electronic and optical properties [13]. Despite remarkable progress made in improving its power conversion efficiency (PCE) over the last decade, the record efficiency

is 10.57% [14], which is still far from the detailed-balance limit of $\sim 30\%$ and performance of other commercial solar cells. A key inhibitor of device performance in Sb_2Se_3 is defect-assisted recombination [15]. Point defects in Sb_2Se_3 have been widely studied by experimental measurements [16–19] and first-principles calculations [20–24]. Defect-detection techniques such as thermal admittance spectroscopy (TAS), deep-level transient spectroscopy (DLTS), and optical deep-level transient spectroscopy (ODLTS) can provide information on defect density and energy levels, whereas the identification of defect atomic identity relies heavily on the theoretically calculated thermodynamic transition level (TL) [25]. Thus, an accurate prediction of defect behavior is essential.

Within the standard procedure of simulating point defects in solids, defect structures are generated by removing, adding, or substituting one atom in an otherwise pristine supercell. Starting from an initial configuration, gradient-based structural relaxation is performed to obtain the defect geometries. However, this approach will find the local minimum configuration *closest* to the initial structure on the potential energy surface (PES), which may not be the ground-state defect structure [26–28]. Metastable structures are thus obtained and the predicted properties are severely affected. The widespread prevalence of this issue has recently been demonstrated [27], and is expected to be exacerbated for systems such as Sb_2Se_3 with low-symmetry crystal structures and flexible bonding environments, which yield complex PESs with many local minima [29].

In this paper, motivated by the observations of valence alternation in chalcogenide semiconductors and advances in global structure searching, we have reinvestigated the accessible charge states and structures of vacancies in Sb_2Se_3 . Going beyond previous theoretical studies, which considered a more limited range of charge states and configurations [20–24], we reveal that both V_{Sb} and V_{Se} are amphoteric, with unconventional stable positive charge states for V_{Sb} and negative charge

*a.walsh@imperial.ac.uk

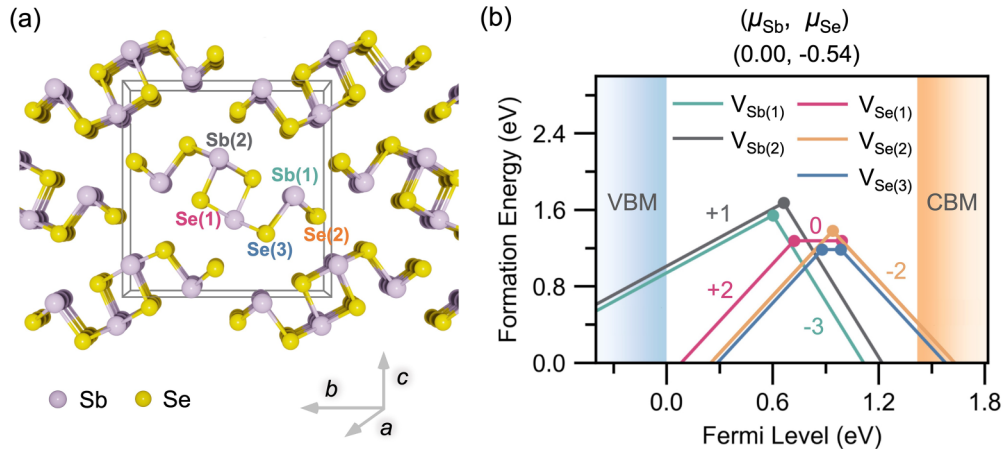


FIG. 1. (a) Crystal structure ($Pnma$ space group) of Sb_2Se_3 . The unit cell is represented by a cuboid. (b) Defect formation energy diagram of V_{Se} and V_{Sb} under Sb-rich equilibrium growth conditions. The slope of the solid line represents the charge state which is shown adjacent to the line. The thermodynamic transition level corresponds to the Fermi-level position where two charged defects have the same formation energies and is given by the solid circle. The valence band maximum (VBM) is set to 0 eV, and the conduction band minimum (CBM) is obtained from the calculated fundamental (indirect) band gap of 1.42 eV by the HSE06 DFT functional.

states for V_{Se} . We predict four-electron negative- U transitions for both Sb and Se vacancies.

II. METHOD

The equilibrium geometric and electronic structures of vacancy defects in Sb_2Se_3 were calculated within the framework of Kohn-Sham density functional theory (DFT) [30,31] as implemented in the Vienna *ab initio* simulation package (VASP) [32]. The projector augmented-wave method [33] was employed with a converged plane-wave energy cutoff of 350 eV. The Heyd-Scuseria-Ernzerhof hybrid functional (HSE06) [34,35] and D3 dispersion correction [36] were used for both the structural relaxation and the static calculation of total energy. The atomic positions were optimized until the Hellman-Feynman forces on each atom were below 0.01 eV/atom. Trial defect configurations were obtained using SHAKENBREAK [27,37] in $3 \times 1 \times 1$ ($11.86 \text{ \AA} \times 11.55 \text{ \AA} \times 11.93 \text{ \AA}$) supercells of the 20-atom conventional unit cell. Here, chemically guided local bond distortions around the defect were employed, alongside random perturbation to all atoms in the supercell, in order to sample the defect PES and identify potential energy-lowering reconstructions. The workflow and comparison to conventional local minimization are provided in Secs. S1, S2, and S4 [38]. The crystal structures were plotted using BLENDER [39] and BEAUTIFUL ATOMS [40]. The formation energy of a defect D in charge state q is defined as [25,41]

$$\Delta E_{D,q}^f = E_{D,q} - E_{\text{host}} + \sum_i n_i \mu_i + qE_F + E_{\text{corr}}, \quad (1)$$

where $E_{D,q}$ and E_{host} are the total energies of the supercell with and without the defect D , respectively. n_i and μ_i indicate the number and the chemical potential of added ($n_i < 0$) or removed ($n_i > 0$) atom of type i , respectively. E_F is the Fermi level and E_{corr} is a correction term for spurious interactions between charged defects under periodic boundary conditions.

The correction scheme developed by Kumagai and Oba [42] which includes anisotropic dielectric screening is used in this work, which has been widely shown to be both accurate and robust [43,44].

III. ACCESSIBLE VACANCY CHARGE STATES IN Sb_2Se_3

As shown in Fig. 1(a), the ground-state crystal structure of Sb_2Se_3 is orthorhombic with quasi-one-dimensional (1D) $[Sb_4X_6]_n$ ribbons stacked together via weak interactions [13]. The unique crystal structure makes it more tolerant to large local lattice deformation compared to conventional crystals with three-dimensional (3D) connectivity. Due to the low crystal symmetry, there are two inequivalent Sb sites and three inequivalent Se sites [shown in Fig. 1(a)], with all sites considered in this work. The defect formation energy diagram in Fig. 1(b) plots the thermodynamically stable charge state as a function of Fermi level in the band gap for vacancy defects in Sb_2Se_3 . As expected, the multiple inequivalent sites with different local environments lead to small but significant differences in the properties of defects of the same type. Anion vacancies are typically positively charged, as the removal of the negatively charged ion from the lattice induces a positive site charge, which can often additionally trap electrons and adopt less negative/neutral charge states. The opposite holds for cation vacancies. In line with previous studies [20–24], 0 and +2 charge states are found to be stable for V_{Se} , and -3 for V_{Sb} . On the other hand, however, abnormally stable *negative* charge states of -2 for V_{Se} (*anion* vacancy) and *positive* $+1$ for V_{Sb} (*cation* vacancy) are also found, revealing strong amphoteric behavior for both V_{Se} and V_{Sb} .

A $(+1/-3)$ charge transition level is observed lying in the middle of the gap for V_{Sb} , regardless of Sb site, indicating that a change in Fermi level will lead to capture or release of four electrons per vacancy. Likewise, a four-electron $(+2/-2)$ TL is found for $V_{Se(2)}$, while $V_{Se(1)}$ and $V_{Se(3)}$ have $(+2/0)$ and

($0/-2$) TLs. Thus both V_{Sb} and V_{Se} are amphoteric negative- U centers, with more typical two-electron negative- U levels in $V_{\text{Se}(1)}$ and $V_{\text{Se}(3)}$ (though exhibiting two such levels each), but rare four-electron transfer levels for $V_{\text{Sb}(1)}$, $V_{\text{Sb}(2)}$, and $V_{\text{Se}(2)}$. We note that our calculated fundamental (indirect) band gap of 1.42 eV is slightly larger than experimental values (1.0–1.2 eV [45–47]), likely due to temperature renormalization [45,48]. However, this should not qualitatively influence our conclusions as all TLs are deep (i.e., near the middle of the band gap). Notably, amphoteric behavior has previously been reported for antisite and interstitial defects in Sb_2Se_3 [21,24], but not for vacancies due to the requirement of structure-searching methods as mentioned above. Thus, our results show that *all* intrinsic defects in Sb_2Se_3 are in fact amphoteric, having the ability to capture both electrons and holes, and yield strong ionic charge compensation.

IV. ELECTRONIC AND STRUCTURAL RECONFIGURATIONS

Negative- U behavior at defects is closely related to lattice distortion and structural reconstruction [6,8,49]. Before examining the defect configurations in detail, let us understand the electronic structure of Sb_2Se_3 . In pristine Sb_2Se_3 , the oxidation states of Sb ($5s^25p^3$) and Se ($4s^24p^4$) are +3 and -2 , respectively, as each Sb cation donates three electrons to the neighboring Se anions, and each Se anion accepts two electrons from the neighboring Sb cations on average. Upon formation of a neutral vacancy defect by removing an atom and its valence electrons, dangling bonds with excess charge in the form of electrons/holes are introduced. Specifically, the removal of Sb with its three donated electrons to create V_{Sb}^0 results in three holes on three Se dangling bonds, while removing Se leaves behind its two accepted electrons with two Sb dangling bonds in V_{Se}^0 . In the fully ionized state (i.e., V_{Sb}^{3-} and V_{Se}^{2+}), electrons are added/removed from the defect site to remove the excess charge and compensate the dangling bonds, stabilizing this charge state. Other charge states can also be stabilized, by localizing the excess charge (e.g., bound small polarons) and/or through atomic rearrangements to form compensating bonds and accommodate the excess charge [49].

Taking V_{Sb} as an example, due to the flexibility of the crystal structure and the tendency to electron pairing for Se species [7], alternative V_{Sb} charge states can be stabilized by the migration of Se anions to form compensating Se-Se bonds at the vacancy. By eliminating the excess holes with this sharing of electrons between dangling bonds, the system energy is lowered. As shown in Fig. 2, the two excess holes in V_{Sb}^- are filled by the formation of a Se-Se dimer, while a Se-Se-Se trimer is formed in V_{Sb}^+ to pair all electrons and fill the four excess holes for this species. V_{Sb}^+ can thus be thought of as a V_{Se}^{2+} - Se_{Sb}^- complex. Such structural reconstruction and negative- U behavior due to paired dangling bonds has previously been termed valence alternation [7], with similar rebonding behavior reported in lone-pair chalcogenide systems [2,6,7,50]. Similarly, a Sb-Sb-Sb trimer is also found in V_{Se}^{2-} , regardless of Se site (Fig. S1 [38]). The formation of an antisite originated from a vacancy in Sb_2Se_3 is also supported by experimental evidence [51], which has found that

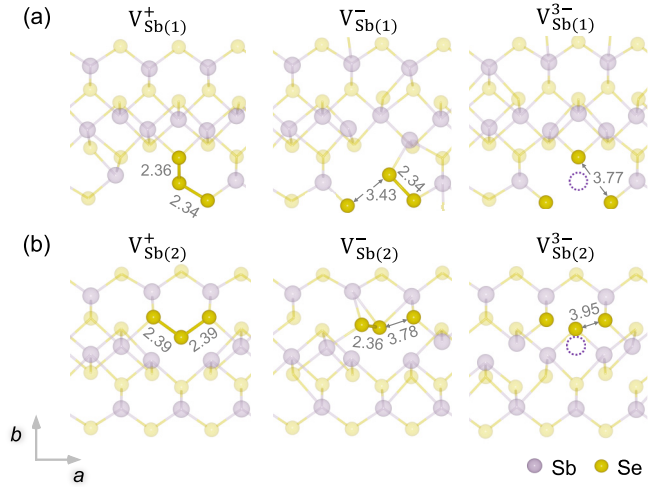


FIG. 2. Local defect geometry of V_{Sb} as a function of charge state. Subscripts (1) and (2) refer to two inequivalent sites. The Se-Se bond lengths are shown in Å, and the vacant Sb site is denoted by a dotted circle.

postannealing treatment facilitates the transformation from V_{Se} to Sb_{Se} by the migration of neighboring Sb cations. All calculated defect structures are shown in Fig. S1 [38].

V. MANY-ELECTRON NEGATIVE- U BEHAVIOR

The difference between positive- and negative- U behavior can be understood through the thermodynamic charge transition levels (TLs). The level $\varepsilon(q_1/q_2)$ is defined as the Fermi-level position where charge states q_1 and q_2 have the same defect formation energies:

$$\varepsilon(q_1/q_2) = \frac{\Delta E_{q_1}^f(E_F = 0) - \Delta E_{q_2}^f(E_F = 0)}{q_2 - q_1}. \quad (2)$$

Let us first assume one defect which can be charged $Q + 1$, Q , or $Q - 1$ depending on the position of the Fermi level, where Q is an arbitrary reference. Two TLs of $\varepsilon(Q + 1/Q)$ and $\varepsilon(Q/Q - 1)$ which define the borders between different charge states are thus considered. The energy separation of the $\varepsilon(Q + 1/Q)$ and $\varepsilon(Q/Q - 1)$ levels from the conduction band minimum (CBM) are the thermodynamic binding energies of the first and second electron to the defect, considering the capture process: $D^{Q+1} + 2e^- \rightarrow D^Q + e^- \rightarrow D^{Q-1}$. The energy difference between these two levels therefore determines the effective correlation energy U_{eff} (cost of trapping an additional charge carrier) [3]:

$$U_{\text{eff}} = \varepsilon(Q/Q - 1) - \varepsilon(Q + 1/Q). \quad (3)$$

Consequently, the sign of U_{eff} depends on the ordering of these TLs. For a typical positive- U center ($U_{\text{eff}} > 0$) [left-hand side of Fig. 3(a)], the position of $\varepsilon(Q + 1/Q)$ lies below $\varepsilon(Q/Q - 1)$, and so D^{Q+1} , D^Q , and D^{Q-1} are each thermodynamically stable for some Fermi level. On the other hand, for a negative- U center ($U_{\text{eff}} < 0$) [right-hand side of Fig. 3(a)], the ordering of $\varepsilon(Q + 1/Q)$ and $\varepsilon(Q/Q - 1)$ is inverted, resulting in a metastable D^Q which would emit charge and decay into D^{Q+1} or D^{Q-1} , depending on E_F . $\varepsilon(Q + 1/Q)$ and

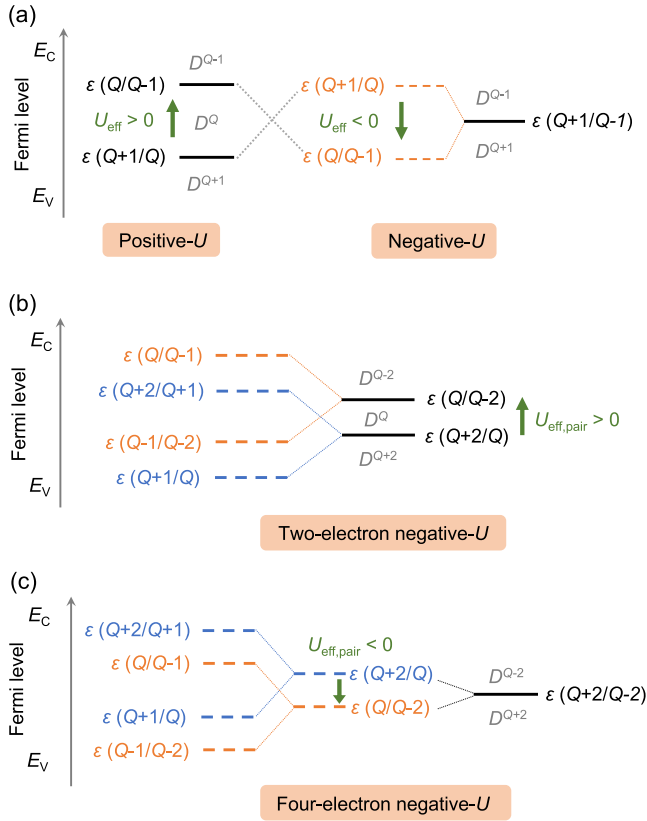


FIG. 3. Schematic diagrams of thermodynamic transition levels for (a) positive- and negative- U centers with three charge states, and (b) two-electron negative- U and (c) four-electron negative- U vacancy centers in Sb_2Se_3 with five charge states. Stable and metastable levels are indicated by solid and dashed horizontal lines, respectively. D^X is the stable defect state under equilibrium conditions at a certain Fermi energy. E_C , conduction band minimum. E_V , valence band maximum.

$\varepsilon(Q/Q - 1)$ are no longer thermodynamically stable TLs, and a single $\varepsilon(Q + 1/Q - 1)$ level appears at the midpoint of these metastable TLs, such that

$$\varepsilon(Q + 1/Q - 1) = \frac{\varepsilon(Q + 1/Q) + \varepsilon(Q/Q - 1)}{2}. \quad (4)$$

Then let us move on to vacancy defects in Sb_2Se_3 . Since the stable TLs within the band gap are $(+2/0)$ and $(0/-2)$, or $(+2/-2)$ for V_{Se} , and $(+1/-3)$ for V_{Sb} [Fig. 1(b)], five charge states $(+1, 0, -1, -2, \text{ and } -3)$ for V_{Sb} , and $(+2, +1, 0, -1, \text{ and } -2)$ for V_{Se} and four corresponding single-electron TLs are possible for both V_{Sb} and V_{Se} . The single-electron TL positions are given in Fig. S2, Tables S2 and S3 [38], with the relative ordering matching that of Fig. 3(b) for the two-electron negative- U centers and Fig. 3(c) for four-electron centers. Here, $Q + 2$, $Q + 1$, Q , $Q - 1$, and $Q - 2$ are used for convenience to explain the general pattern, where Q equals -1 for V_{Sb} and 0 for V_{Se} . As shown in Fig. 1(b) and depicted in Figs. 3(b) and 3(c), for all cases in V_{Sb} and V_{Se} , the transitions of $D^{Q+2} \rightarrow D^{Q+1} \rightarrow D^Q$ (shown in blue dashed lines in Fig. 3) and $D^Q \rightarrow D^{Q-1} \rightarrow D^{Q-2}$ (shown in orange dashed lines) show negative- U ordering and thus a two-electron transition for both $D^{Q+2} \rightarrow D^Q$ and $D^Q \rightarrow D^{Q-2}$. Here, for such

cases with double two-electron TLs, we define an effective electron-pair correlation energy $U_{\text{eff,pair}}$ —analogous to U_{eff} for single-electron correlation—which corresponds to the energy cost of trapping an additional charge carrier pair:

$$U_{\text{eff,pair}} = \varepsilon(Q/Q - 2) - \varepsilon(Q + 2/Q). \quad (5)$$

The relative positions of the $\varepsilon(Q/Q - 2)$ and $\varepsilon(Q + 2/Q)$ negative- U levels then dictate whether the defect is a two-electron or four-electron center. If $\varepsilon(Q + 2/Q)$ lies below $\varepsilon(Q/Q - 2)$ [Fig. 3(b)], a center with two typical two-electron negative- U levels ($U_{\text{eff,pair}} > 0$) is formed. This is the case for $V_{\text{Se}(1)}$ and $V_{\text{Se}(3)}$ with $U_{\text{eff,pair}}$ of 0.27 and 0.11 eV, respectively. If on the other hand the ordering of these two levels are inverted once again [Fig. 3(c)], the defect would show a four-electron transfer behavior ($U_{\text{eff,pair}} < 0$) with the largest binding energy for the fourth electron, resulting in only two thermodynamically stable charge states D^{Q+2} and D^{Q-2} within the band gap. This is the case for $V_{\text{Sb}(1)}$, $V_{\text{Sb}(2)}$, and $V_{\text{Se}(2)}$, with negative $U_{\text{eff,pair}}$ values of -0.28 , -0.09 , and -0.04 eV, respectively, thus showing four-electron negative- U behavior. However, we note that the prediction of four-electron transfer behavior here is based on a thermodynamic perspective. The kinetics of each single-electron transition are discussed in more detail in Sec. S5 [38].

Substantial structural relaxation is necessary to realize negative- U behavior [2,5]. While a four-electron negative- U transition is found for both sites in V_{Sb} , in V_{Se} it depends on the Se site. Only $V_{\text{Se}(2)}$ shows a four-electron negative- U behavior and the other sites show a two-electron one. The two- or four-electron negative- U behavior (i.e., the sign of $U_{\text{eff,pair}}$) of vacancies in Sb_2Se_3 depends on the thermodynamic stability of the middle point D^Q with respect to the extremal charged defects ($D^{Q\pm 2}$). To quantify the effect of structural deformation on defect stability, we calculate the relaxation energy of each charge state in V_{Sb} and V_{Se} (Sec. S6 [38]), which is defined as the energy difference between unrelaxed and relaxed defect configurations. Larger relaxation energies for $D^{Q\pm 2}$ than D^Q are more likely to yield a metastable D^Q and thus a four-electron negative- U level, as witnessed for V_{Se} (Table S8 [38]). This indicates the key role of structural reconstruction in determining the negative- U properties of these defect species.

VI. SUMMARY

In summary, structural configurations and electronic properties of vacancy defects in Sb_2Se_3 have been systematically modeled using a global search procedure. Both types of vacancies are amphoteric, with strong self-charge compensation, and show either two- or four-electron negative- U behavior depending on the atomic site. These phenomena are linked to structural reconstruction in V_{Sb}^+ and V_{Se}^{2-} , facilitated by the formation of Se/Sb trimers to pair electrons and compensate dangling bonds. The ability to reconstruct and thus stabilize unusual defect charge states is attributed to the structural flexibility of Sb_2Se_3 and the valence alternation of Se and Sb species, and thus could be present in related low-dimensional chalcogenide semiconductors such as SbSeI or CuSbSe_2 .

ACKNOWLEDGMENTS

For computational resources we are grateful to the U.K. Materials and Molecular Modelling Hub and the U.K.'s HEC Materials Chemistry Consortium, which are funded by UKRI (EPSRC Grants No. EP/T022213/1 and No.

EP/L000202). X.W. acknowledges Imperial College London for support via a President's Ph.D. Scholarship. S.R.K. acknowledges the EPSRC Centre for Doctoral Training in the Advanced Characterisation of Materials (EP/S023259/1) for support via a Ph.D. studentship.

- [1] S. T. Pantelides, *Rev. Mod. Phys.* **50**, 797 (1978).
- [2] K. W. Boer and U. W. Pohl, *Semiconductor Physics* (Springer, Berlin, 2018), Chap. 5.
- [3] G. D. Watkins, in *Advances in Solid State Physics*, edited by P. Grosse (Springer, Berlin, 1984), Vol. 24, pp. 163–189.
- [4] J. Hubbard, *Proc. R. Soc. London, Ser. A* **276**, 238 (1963).
- [5] P. Anderson, *Phys. Rev. Lett.* **34**, 953 (1975).
- [6] R. Street and N. Mott, *Phys. Rev. Lett.* **35**, 1293 (1975).
- [7] M. Kastner, D. Adler, and H. Fritzsche, *Phys. Rev. Lett.* **37**, 1504 (1976).
- [8] J. Coutinho, V. P. Markevich, and A. R. Peaker, *J. Phys.: Condens. Matter* **32**, 323001 (2020).
- [9] G. A. Baraff, E. O. Kane, and M. Schlüter, *Phys. Rev. Lett.* **43**, 956 (1979).
- [10] J. R. Troxell and G. D. Watkins, *Phys. Rev. B* **22**, 921 (1980).
- [11] C. G. Hemmingsson, N. T. Son, A. Ellison, J. Zhang, and E. Janzén, *Phys. Rev. B* **58**, R10119 (1998).
- [12] H. C. Alt, *Phys. Rev. Lett.* **65**, 3421 (1990).
- [13] X. Wang, Z. Li, S. R. Kavanagh, A. M. Ganose, and A. Walsh, *Phys. Chem. Chem. Phys.* **24**, 7195 (2022).
- [14] Y. Zhao, S. Wang, C. Li, B. Che, X. Chen, H. Chen, R. Tang, X. Wang, G. Chen, T. Wang *et al.*, *Energy Environ. Sci.* **15**, 5118 (2022).
- [15] J. Dong, Y. Liu, Z. Wang, and Y. Zhang, *Nano Select* **2**, 1818 (2021).
- [16] W. Lian, R. Cao, G. Li, H. Cai, Z. Cai, R. Tang, C. Zhu, S. Yang, and T. Chen, *Adv. Sci.* **9**, 2105268 (2022).
- [17] X. Hu, J. Tao, G. Weng, J. Jiang, S. Chen, Z. Zhu, and J. Chu, *Sol. Energy Mater. Sol. Cells* **186**, 324 (2018).
- [18] X. Wen, C. Chen, S. Lu, K. Li, R. Kondrotas, Y. Zhao, W. Chen, L. Gao, C. Wang, J. Zhang *et al.*, *Nat. Commun.* **9**, 2179 (2018).
- [19] T. D. Hobson, L. J. Phillips, O. S. Hutter, K. Durose, and J. D. Major, *Appl. Phys. Lett.* **116**, 261101 (2020).
- [20] X. Liu, X. Xiao, Y. Yang, D. Xue, D. Li, C. Chen, S. Lu, L. Gao, Y. He, M. C. Beard *et al.*, *Prog. Photovoltaics: Res. Appl.* **25**, 861 (2017).
- [21] C. N. Savory and D. O. Scanlon, *J. Mater. Chem. A* **7**, 10739 (2019).
- [22] M. Huang, P. Xu, D. Han, J. Tang, and S. Chen, *ACS Appl. Mater. Interfaces* **11**, 15564 (2019).
- [23] A. Stolaroff, A. Lecomte, O. Rubel, S. Jobic, X. Zhang, C. Latouche, and X. Rocquefelte, *ACS Appl. Energy Mater.* **3**, 2496 (2020).
- [24] M. Huang, Z. Cai, S. Wang, X.-G. Gong, S.-H. Wei, and S. Chen, *Small* **17**, 2102429 (2021).
- [25] C. Freysoldt, B. Grabowski, T. Hickel, J. Neugebauer, G. Kresse, A. Janotti, and C. G. Van de Walle, *Rev. Mod. Phys.* **86**, 253 (2014).
- [26] I. Mosquera-Lois and S. R. Kavanagh, *Matter* **4**, 2602 (2021).
- [27] I. Mosquera-Lois, S. R. Kavanagh, A. Walsh, and D. O. Scanlon, *npj Comput. Mater.* **9**, 25 (2023).
- [28] A. Kononov, C.-W. Lee, E. P. Shapera, and A. Schleife, *J. Phys.: Condens. Matter* **35**, 334002 (2023).
- [29] S. R. Kavanagh, D. O. Scanlon, A. Walsh, and C. Freysoldt, *Faraday Discuss.* **239**, 339 (2022).
- [30] W. Kohn and L. J. Sham, *Phys. Rev.* **140**, A1133 (1965).
- [31] R. M. Dreizler and E. K. Gross, in *Density Functional Theory* (Springer, Berlin, 1990), pp. 245–271.
- [32] G. Kresse and J. Furthmüller, *Phys. Rev. B* **54**, 11169 (1996).
- [33] G. Kresse and D. Joubert, *Phys. Rev. B* **59**, 1758 (1999).
- [34] J. Heyd, G. E. Scuseria, and M. Ernzerhof, *J. Chem. Phys.* **118**, 8207 (2003).
- [35] A. V. Krukau, O. A. Vydrov, A. F. Izmaylov, and G. E. Scuseria, *J. Chem. Phys.* **125**, 224106 (2006).
- [36] S. Grimme, *J. Comput. Chem.* **25**, 1463 (2004).
- [37] I. Mosquera-Lois, S. R. Kavanagh, A. Walsh, and D. O. Scanlon, *J. Open Source Softw.* **7**, 4817 (2022).
- [38] See Supplemental Material at <http://link.aps.org/supplemental/10.1103/PhysRevB.108.134102> for the workflow of defect geometry optimization; checks for cases with trimer formation; geometries and formation energies of V_{Sb} and V_{Se} ; comparison of global and local searches; potential energy surfaces; relaxation energies of V_{Sb} and V_{Se} .
- [39] Blender Online Community, *Blender - A 3D Modelling and Rendering Package*, Blender Foundation, Stichting Blender Foundation, Amsterdam, 2018, <http://www.blender.org>.
- [40] X. Wang, T. Tian, and A. Ulrich, Beautiful Atoms: A Python library for the manipulation and visualization of atomistic structure using Blender, 2022, <https://github.com/beautiful-atoms/beautiful-atoms> (accessed on 1st June 2022).
- [41] S. B. Zhang and J. E. Northrup, *Phys. Rev. Lett.* **67**, 2339 (1991).
- [42] Y. Kumagai and F. Oba, *Phys. Rev. B* **89**, 195205 (2014).
- [43] A. Walsh, *npj Comput. Mater.* **7**, 72 (2021).
- [44] F. Oba and Y. Kumagai, *Appl. Phys. Express* **11**, 060101 (2018).
- [45] F. Kosek, J. Tulka, and L. Štourač, *Czech. J. Phys. B* **28**, 325 (1978).
- [46] C. Chen, K. Li, and J. Tang, *Solar RRL* **6**, 2200094 (2022).
- [47] K. Zeng, D.-J. Xue, and J. Tang, *Semicond. Sci. Technol.* **31**, 063001 (2016).
- [48] Y. Liu, J. Wiktor, and B. Monserrat, *Phys. Rev. Mater.* **7**, 085401 (2023).
- [49] S. R. Kavanagh, A. Walsh, and D. O. Scanlon, *ACS Energy Lett.* **6**, 1392 (2021).
- [50] A. Kolobov, *J. Non-Cryst. Solids* **198-200**, 728 (1996).
- [51] B. Che, Z. Cai, P. Xiao, G. Li, Y. Huang, R. Tang, C. Zhu, S. Yang, and T. Chen, *Adv. Mater.* **35**, 2208564 (2023).